J Appl Electrochem (2009) 39:727–736
DOI 10.1007/s10800-008-9716-y

ORIGINAL PAPER

Comparative electrocatalytic behavior of self-assembled monolayer of thiol derivatised Co (II) phthalocyanines on gold disk, ultramicro cylinder and fiber electrodes

Nolwazi Nombona · Daniela A. Geraldo · Jean Hakuzimana · Anne Schwarz · Philippe Westbroek · Tebello Nyokong

Received: 14 August 2008 / Accepted: 5 November 2008 / Published online: 22 November 2008
© Springer Science+Business Media B.V. 2008

Abstract This paper reports on the use of thiol derivatised cobalt phthalocyanines as self assembled monolayers (SAMs) on gold disk electrode, gold ultramicro-cylinder electrode (UMCE) and on gold coated fiber for the detection of L-cysteine. The complexes are peripherally and non-peripherally substituted with phenylthio substituents. The SAM modified electrodes showed enhancement of catalytic currents and overpotential reduction occurred on the gold modified electrodes with different geometries. Electrocatalytic oxidation of L-cysteine on SAM modified gold coated fiber was reported for the first time. The gold coated fiber and ultramicro cylinder electrode were less stable towards the electrocatalytic oxidation of cysteine compared to its oxidation on the gold disk. The gold disk electrode gave better catalytic performance in terms of stability and reduction of overpotential.

Keywords Cobalt phthalocyanine · Self assembled monolayer · Gold ultramicro cylinder · Gold coated fiber · L-cysteine oxidation · Electrocatalysis

1 Introduction

Metallophthalocyanines (MPcs) have gained a lot of attention due to their versatility which includes electrochemical sensing, semi-conduction, non-linear optics and photodynamic therapy [1–11]. MPcs that are synthesized to contain sulfur groups may be used for the formation of self assembled monolayer (SAM). SAMs have become an intelligent approach for the modification of gold or silver surfaces as they provide a defined and controlled composition on the electrode surface [12, 13]. SAM formation occurs as a consequence of spontaneous adsorption of a thiol molecule to a gold surface to give a monomolecular layer on the surface. SAM modified electrodes are useful for practical applications such as chemical sensing, bioelectronic devices and for controlling surface properties like corrosion and wettability [14].

In this work, three gold electrodes with different geometries were used for SAM formation. The electrodes are: a gold disk, gold ultramicro-cylinder and a gold coated fiber electrodes. Ultramicroelectrodes (UMEs) are electrodes that have dimensions of a few micrometers and are characterized by high mass transport, reduced capacitance and resistance [15–18]. Using a coated textile fiber is a new way of making a gold electrode from textiles. Textiles have gained a lot of interest for use as electrotextiles due to their potential use for micro-filtration, medical and military uses. Electrotextiles are fibers, yarns or garments that can conduct an electrical current. In this work, the para-aramide fiber used was chemically deposited with conductive material (poly-pyrole, copper and gold consecutively) such that the surface of the fiber became conductive [19]. MPc-SAMs' were formed for the first time on the gold coated fibers and were employed for the detection of L-cysteine. The MPc complexes employed in this work are the CoPc derivatives: cobalt 1,(4)-(tetraphenylthiophthalocyaninato) (**1**) and cobalt 2,(3)-(tetraphenylthiophthalocyaninato) (**2**), Fig. 1 [20].

L-cysteine is a non-essential amino acid formed from serine and methionine in the body. High levels of this amino acid results in diseases such as Alzheimer's and

N. Nombona · D. A. Geraldo · T. Nyokong (✉)
Department of Chemistry, Rhodes University, P. O. Box 94, Grahamstown 6140, South Africa
e-mail: t.nyokong@ru.ac.za

N. Nombona · J. Hakuzimana · A. Schwarz · P. Westbroek
Department of Textiles, Ghent University, Technologiepark 907, 9052 Gent, Belgium

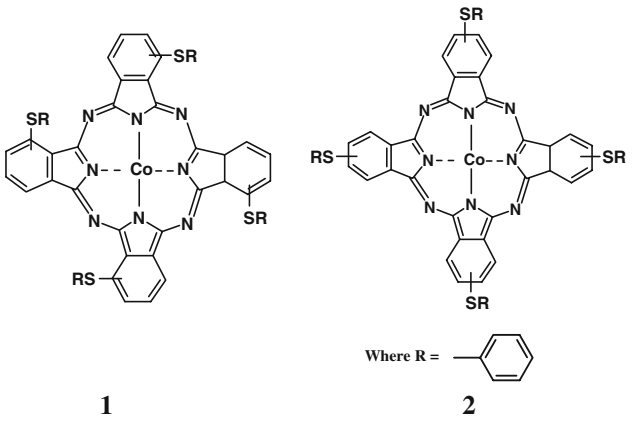

Fig. 1 Structure of CoPc derivatives: cobalt 1,(4)-tetraphenylthiophthalocyaninato) (**1**) and cobalt 2,(3)-(tetraphenylthiophthalocyaninato) (**2**)

Parkinson's diseases [21, 22] as well as epileptic seizures [23] whereas low levels are linked to a high risk of cervical dysphasia [24]. Incorrect levels of the amino acid in the body may also cause an autoimmune deficiency syndrome [25]. The importance of this amino acid in biological systems makes its detection to be of paramount importance.

2 Experimental

2.1 Materials

L-cysteine, dimethylformamide (DMF), KOH, Na_2SO_4, $HClO_4$, $Fe(NH_4)(SO_4)_2$, H_2SO_4 and pH 4 buffer tablets were purchased form Sigma-Aldrich. The syntheses and characterization of the CoPc derivatives: cobalt 1,(4)-(tetraphenylthiophthalocyaninato) (**1**) and cobalt 2,(3)-(tetraphenylthiophthalocyaninato) (**2**) have been reported elsewhere [20]. All solvents used for electrochemical experiments were freshly distilled and deaerated by bubbling argon before use and the electrochemical set-up was kept under argon atmosphere throughout the experiments, other reagents were used as received. Fresh L-cysteine solutions were prepared before use and were deaerated with argon as cysteine can be oxidized to cystine by atmospheric oxygen.

Gold ultramicro wire was purchased from Goodfellow Metals Ltd., UK, Teflon was purchased from Stokvis Plastics, Belgium and the gold coated fibers were prepared according to the in-house developed procedures [26, 27] at the Department of Textiles, Gent University.

2.2 Electrochemical methods

Cyclic voltammetry (CV) experiments were carried using the Autolab potentiostat PGSTAT 30 (Eco Chemie, Utrecht, The Netherlands) using the General Purpose Electrochemical System data processing software (GPES, version 4.9) or Advanced Electrochemical System (Princeton Applied Research) PAR-STAT 2273 equipment. A three electrode set-up was employed. The working electrodes were unmodified Au disk ($r = 0.2$ mm) from BioAnalytical Systems), Au ultra microelectrode cylinder wire ($d = 25$ μm) or Au coated fiber electrodes (each strand $d = 9$ μm), or these electrodes modified with SAMs of complexes **1** and **2**, to form MPc-SAMs. A standard Ag|AgCl (saturated KCl) was used as a reference electrode and a platinum wire as the counter electrode. Rotating disk electrode voltammetry was carried out using a BioAnaylytical System (BAS) model 100B/W Electrochemical Workstation.

2.3 Fabrication of gold ultramicro cylinder and fiber electrodes

The gold ultramicro cylinder electrode (UMCE) was constructed by using a 3 cm long and 0.5 cm wide Teflon block. A 1 mm gap was made along the width at the bottom end of the block. A small hole was made 0.5 cm from the top of the plate to allow for the insertion of a copper wire which served as a connection to the electrochemistry system. The ultramicro wire or the gold coated fiber was then coiled around the copper wire (for contact) and the sides of the block, and then positioned over the gap at the bottom of the block, exposing 1 mm fiber (the working part of the electrode). The electrodes were used for SAM formation. After the SAM had been formed the UMCE or gold coated fiber was rinsed in DMF followed by Millipore water, once dry, epoxy glue was used to cover the UMCE or gold coated fiber only exposing the 1 mm surface on which the SAM was formed.

2.4 Formation of self-assembled monolayers

The gold disk electrode was polished with slurries of 0.05 μm alumina on a SiC-emery paper, thereafter the electrode was sonicated in ethanol for 1 h to remove residual alumina particles. The gold electrode was then immersed in a hot piranha solution (1:3, v/v, 30% H_2O_2 and concentrated H_2SO_4) to remove organic particles that may still be on the electrode surface. The electrode was then rinsed in Millipore water and then with distilled DMF. The gold UMCE was sonicated in ethanol for 1 h and then it underwent oxidative cleaning using linear sweep voltammetry scans from –1.5 to 1.5 V, the same was done for the gold coated fiber. The hot piranha solution could not be used as it would have destroyed the UMCE and the gold coated fiber. The gold coated fiber and the UMCE were then rinsed with Millipore water followed by distilled

DMF. Following this treatment, the bare gold disk electrode, gold UMCE and gold coated fiber electrodes were immersed in argon-purged 1 10^{-6} mol cm^{-3} solutions of the MPc (complexes **1** or **2**). The SAMs are represented as **1**-SAM or **2**-SAM for complexes **1** and **2**. The SAM's were allowed to form for 48 h on the disk electrode, 1 h on the gold UMCE as well as on the gold coated fiber. The modified electrodes were first rinsed in DMF to remove any adsorbed species and then rinsed with Millipore water before use.

Atomic force microscopy (AFM) images were recorded in the non-contact mode in air with a CP-11 Scanning Probe Microscope from Veeco Instruments (Carl Zeiss, South Africa) at a scan rate of 1 Hz. A gold coated crystal (Q-Sense®, Sweden) was used for the formation of SAM.

3 Results and discussion

3.1 Self-assembled monolayer characterization: Au disk electrode

A gold surface which is well covered with a self-assembled monolayer should block Faradic process that would easily occur at the bare gold surface, such processes include the blockage of gold oxidation/reduction which occurs when oxygen is present in solution and the blockage of the $\left[Fe(H_2O)_6\right]^{3+}/\left[Fe(H_2O)_6\right]^{2+}$ couple. We studied the gold electrode behavior in acid media (Na_2SO_4, pH 4), basic media (1×10^{-5} mol cm^{-3} KOH), in 1×10^{-6} mol cm^{-3} $Fe(NH_4)(SO_4)_2$ in 2×10^{-4} mol cm^{-3} $HClO_4$ and in 1×10^{-6} mol cm^{-3} $K_3Fe(CN)_6$ in 2×10^{-4} mol cm^{-3} KCl.

Figure 2a shows the CV of the bare gold disk electrode and the MPc-SAM modified gold disk electrodes in 1×10^{-6} mol cm^{-3} Na_2SO_4 (pH 4). Both **1**-SAM and **2**-SAM modified electrodes show reduction in charging currents in Fig. 2a, confirming modification of the electrode. The Co^{III}/Co^{II} process is known to be difficult and if found irreversible for adsorbed CoPc complexes, often showing no anodic component at all [28]. Figure 2b shows that complex **1**-SAM exhibits more blockage of the gold oxidation/reduction process in 1×10^{-5} mol cm^{-3} KOH compared to complex **2**-SAM which still shows the presence of gold oxide peaks (though small) even after modification, hence suggesting larger ion permeability for the latter. The broad peaks between +0.25 and 0.4 V are most probably due to the $Co^{III}Pc^{-2}/Co^{II}Pc^{-2}$ process, in comparison with literature for adsorbed thio substituted CoPc complexes [29, 30]. Figure 2c shows the inhibition of the $\left[Fe(H_2O)_6\right]^{3+}/\left[Fe(H_2O)_6\right]^{2+}$ redox process in the presence of SAMs. The peaks near 0.7 V are due to MPc based redox processes. The $\left[Fe(H_2O)_6\right]^{3+}/\left[Fe(H_2O)_6\right]^{2+}$ redox process is a known reversible process of $Fe(NH_4)(SO_4)_2$ solution at bare gold electrodes, SAM modification of gold electrodes results in this process being inhibited.

The fast electron transfer of the $\left[Fe(CN)_6{}^{3-}\right]/\left[Fe(CN)_6{}^{4-}\right]$ redox couple is not inhibited by the SAM's as shown in Fig. 2d as compared to the $\left[Fe(H_2O)_6\right]^{3+}/\left[Fe(H_2O)_6\right]^{2+}$ redox process (Fig. 2c), but the cathodic to

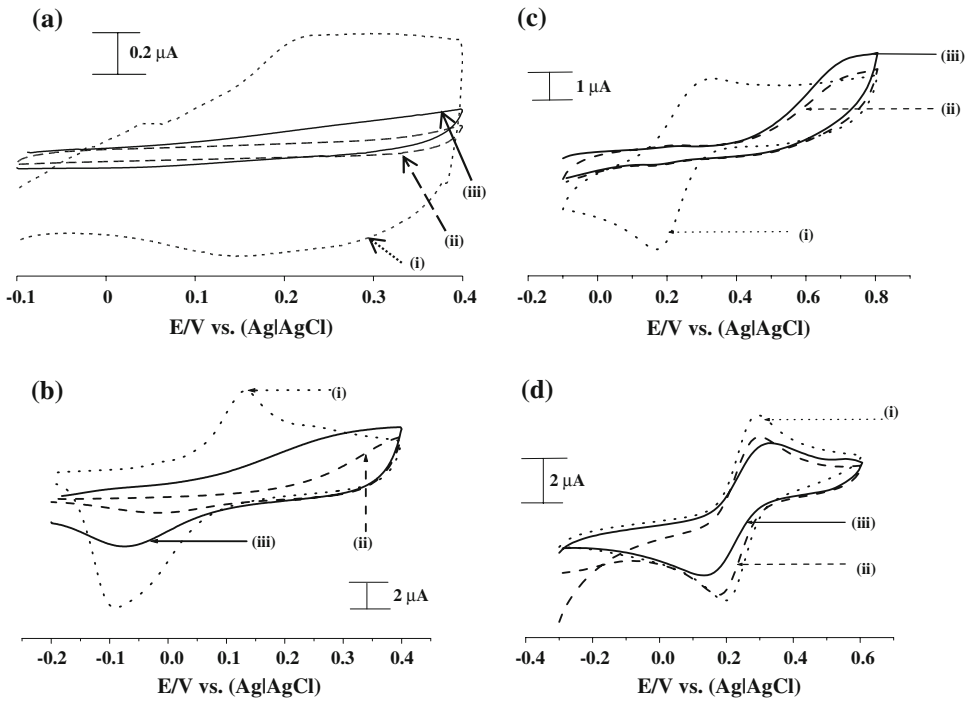

Fig. 2 Cyclic voltammograms of (i, dotted) unmodified gold disk electrode, (ii, dashed) SAM of complex **1** and (iii, solid) SAM of complex **2** in (**a**) 1×10^{-6} mol cm^{-3} Na_2SO_4 in pH 4 buffer solution, (**b**) 1×10^{-5} mol cm^{-3} KOH solution, (**c**) 1×10^{-6} mol cm^{-3} $Fe(NH_4)(SO_4)_2$ in 2×10^{-4} mol cm^{-3} $HClO_4$ solution, (**d**) 1×10^{-6} mol cm^{-3} $K_3Fe(CN)_6$ in 2×10^{-4} mol cm^{-3} KCl solution. Scan rate = 50 mV s^{-1}

anodic peak potential separation (ΔE) for this couple increases for SAM modified electrodes. The lack of inhibition of $[Fe(CN)_6^{3-}]/[Fe(CN)_6^{4-}]$ redox couple has been observed before using adsorbed cobalt tetra-aminophthalocyanine films on vitreous carbon electrodes [31]. It was reported [31] that both modified and unmodified electrodes showed the same redox potential and almost equal peak currents intensities for the $[Fe(CN)_6^{3-}]/[Fe(CN)_6^{4-}]$ redox reaction, and that the modified electrodes act as electronic conductors which allow rapid electron transfer to the solution species [31]. The lack of inhibition for this couple was also observed for MnPc-SAMs [29].

Surface coverage (Γ_{MPc}, mol/cm^2) of complexes on the gold disk electrodes were estimated using Eq. 1:

$$\Gamma_{MPc} = \frac{Q}{n\ FA} \quad (1)$$

where Q is the background corrected electric charge under the anodic peaks (at 0.3 V for **1** and 0.4 V for **2**) of the SAM modified electrode in pH 4 buffer solution (Fig. 3 showing the Co^{III}/Co^{II} peak for complex **1** and **2**), n is the number of electrons transferred (assume $\approx$ 1), F is the Faraday constant (96485 C/mol) and A is the surface area of the electrode (0.02011 cm^2). The surface coverage for complex **1** and for complex **2** was estimated to be 1.35×10^{-10} mol cm^{-2} and 1.04×10^{-10} mol cm^{-2} respectively. These values are close to the expected value (1×10^{-10} mol cm^{-2}) for a phthalocyanine monolayer lying flat on a surface [32], confirming a monolayer formation of the phthalocyanine on the electrode surface.

The ion blocking factor, often called ion barrier factor (Γ_{ibf}) was calculated using Eq. 2 to give an indication of the solvent or ion permeability of the SAM's, the ideal value of $\Gamma_{ibf} = 1$, indicates the SAM's ability to block ions

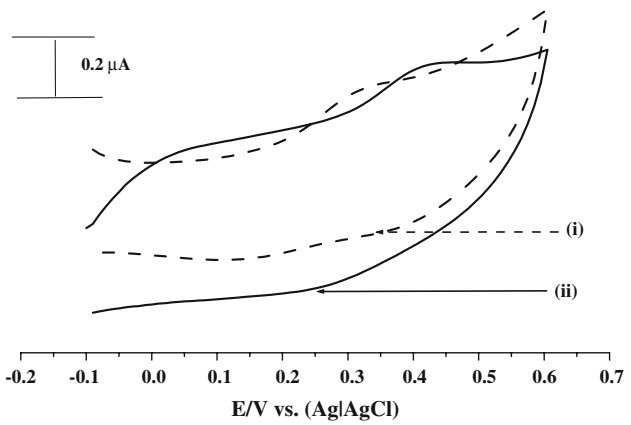

Fig. 3 Cyclic voltammogram of (i) SAM of complex **1** and (ii) SAM of complex **2** (on Au disk electrode) in pH4 buffer solution, observed after several cycles

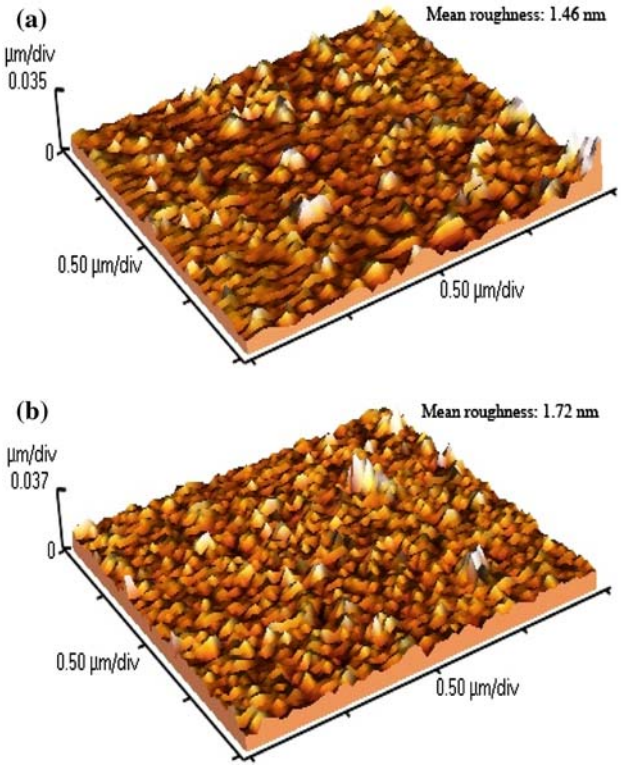

Fig. 4 AFM images of (**a**) bare Au and (**b**) 1-SAM

or solvent from penetrating the surface of the electrode [33].

$$\Gamma ibf = 1 - \left(\frac{Q_{SAM}}{Q_{Bare}}\right) \quad (2)$$

where Q_{SAM} and Q_{BARE} is charge under the cathodic peaks in 1×10^{-5} mol cm^{-3} KOH solution (Fig. 2b) for **1**-SAM (or **2**-SAM) and bare solid disk electrodes respectively. For complex **1**, Γ_{ibf} was calculated to be 0.96 and $\Gamma_{ibf} = 0.82$ for complex **2**-SAM. This shows that both SAM's have a relatively good barrier with minimum defects with complex **1**-SAM being the better monolayer.

AFM images (Fig. 4) of the **1**-SAM or **2**-SAM are similar to other SAM electrodes reported before [34], showing an increase in roughness upon formation of SAM.

3.2 Self-assembled monolayer characterization: Au ultramicro cylinder (UMCE) and gold coated fiber electrodes

The cyclic voltammetry of the bare Au UMCE in 1×10^{-6} mol cm^{-3} Na_2SO_4 (pH 4) solution is shown in Fig. 5a. The MPc-SAM modified Au UMCEs show huge reduction in charging currents as observed above for the Au disk electrode, confirming the modification of the electrode. The $Co^{III}Pc^{-2}/Co^{II}Pc^{-2}$ oxidation process is

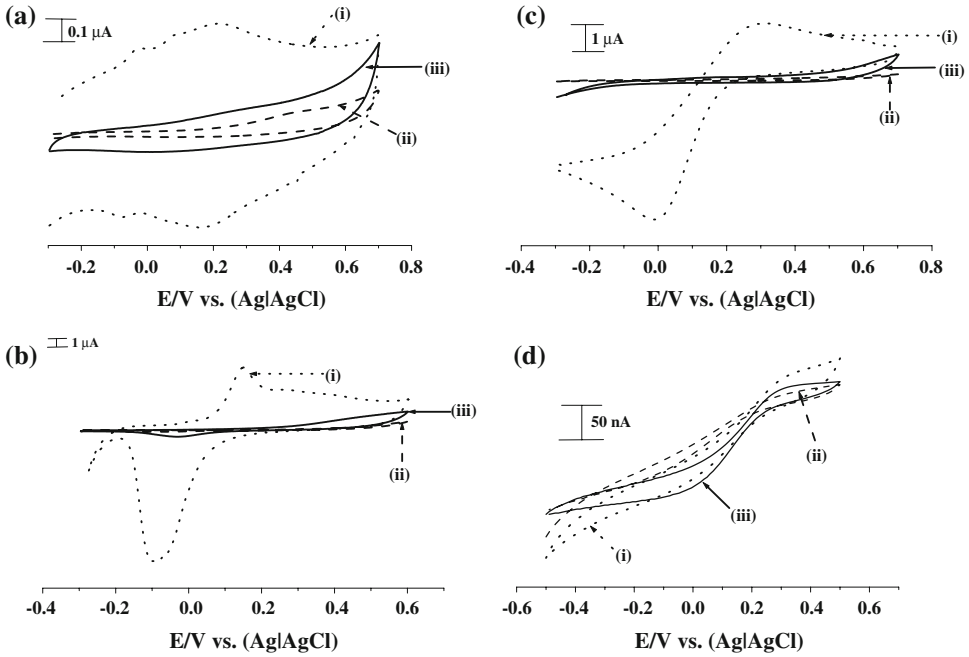

Fig. 5 Cyclic voltammograms of (i, dotted) unmodified gold UMCE, (ii, dashed) SAM of complex **1** and (iii, solid) SAM of complex **2** in (**a**) 1×10^{-6} mol cm^{-3} Na_2SO_4 in pH 4 buffer solution, (**b**) 1×10^{-5} mol cm^{-3} KOH solution, (**c**) 1×10^{-6} mol cm^{-3} $Fe(NH_4)(SO_4)_2$ in 2×10^{-4} mol cm^{-3} $HClO_4$ solution, (**d**) 1×10^{-6} mol cm^{-3} $K_3Fe(CN)_6$ in 2×10^{-4} mol cm^{-3} KCl solution. Scan rate = 50 mV s^{-1}

observed for complex **1**-SAM as a very weak peak around 0.4 V, and is not very clear for **2**-SAM.

Figure 5b shows the blockage of Au oxidation/reduction on the UMCE in 1×10^{-5} mol cm^{-3} KOH solution. A pronounced redox process was observed on the bare electrode, with a weaker anodic process. The SAM modified electrodes show greatly reduced currents. The SAM's were investigated for the suppression of the $\left[Fe(H_2O)_6\right]^{3+}/\left[Fe(H_2O)_6\right]^{2+}$ Faradic process, Fig. 5c. The MPc-SAM modified electrodes show complete inhibition of the oxidation process. The SAM modified UMCEs were studied in 1×10^{-6} mol cm^{-3} $K_3Fe(CN)_6$ in 2×10^{-4} mol cm^{-3} KCl, Fig. 5d, sigmoidal shaped potential curves which are typical of UMCEs are observed. The rate of diffusion of the $\left[Fe(CN)_6^{3-}\right]$ species to the electrode surface is very fast hence steady-state currents are reached quickly and the voltammetric response is sigmaiodal. The lack of blockage of the $\left[Fe(CN)_6{}^{3-}\right]/\left[Fe(CN)_6{}^{4-}\right]$ redox couple may be explained as discussed above for the Au disc electrode.

The Γ_{ibf} values were calculated (using Fig. 5b) for **1**-SAM and **2**-SAM to be 0.97 and 0.95, respectively. Table 1 shows the SAMs of **1** and **2** on Au UMCE had less defects (for **2**-SAM) and almost similar defects (for **1**-SAM) than the disk electrode, where the Γ_{ibf} values were 0.96 (**1**-SAM) and 0.82 (**2**-SAM).

For the Au fiber electrode, the blockage of the Au redox processes also occurred in 1×10^{-5} mol cm^{-3} KOH as shown in Fig. 6. The Γ_{ibf} values were determined (using Fig. 6) for **1**-SAM and **2**-SAM to be 0.88 for both SAMs. This indicates that the SAMs have the same permeability. Table 1, shows the **1**-SAM and **2**-SAM have more defects on fiber electrodes (smaller Γ_{ifb}, Table 1) than on UMCEs, and more (for **1**-SAM) and slightly less defects (for **2**-SAM) defects than Au disk electrode.

The UMCE gives better Γ_{ibf} values than the other two types of electrodes, suggesting that the SAM on the UMCE has less pinholes compared to the SAMs on the other electrode geometries.

3.3 L-Cysteine oxidation

The cysteine concentration of 1×10^{-6} mol cm^{-3} was employed for all electrodes for comparison purposes. Figure 7a shows cyclic voltammograms of pH 4 buffer solution containing 1×10^{-6} mol cm^{-3} of L-cysteine on bare and SAM modified Au disk electrodes using

Table 1 Electrochemical parameters for the SAMs of complexes **1** and **2** on the various Au electrodes and for L-cysteine detection

Parameter	Au disk		Au UMCE		AU fiber	
	Complex **1**	Complex **2**	Complex **1**	Complex **2**	Complex **1**	Complex **2**
Γ_{ifb}	0.96	0.82	0.97	0.95	0.88	0.88
Cysteine oxidation V (versus Ag|AgCl) in 1×10^{-6} mol cm^{-3} solution	0.55	0.65	0.84	0.90	0.77	0.62

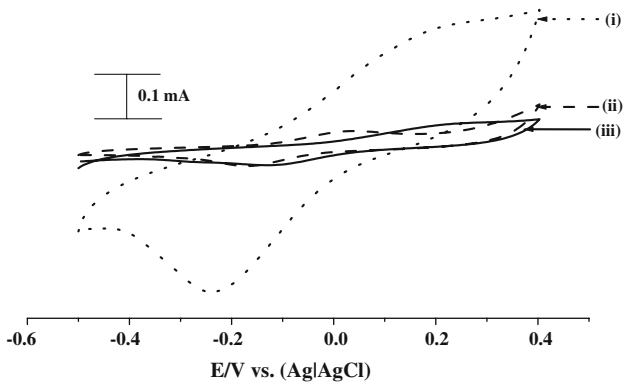

Fig. 6 Cyclic voltammograms of (i, dotted) unmodified gold fiber coated electrode, (ii, dashed) SAM of complex **1** and (iii, solid) SAM of complex **2** in 1×10^{-5} mol cm^{-3} KOH solution. Scan rate = 50 mV s^{-1}

complexes **1** and **2**. The bare electrode shows no clear cysteine oxidation peak. Clear peaks [at 0.55 V (for **1**) and 0.65 V (for **2**)] and a large increase in currents are observed due to catalytic cysteine oxidation on SAMs of both complexes **1** and **2**. The potential value for cysteine oxidation on these electrodes is more positive than was reported for FePc SAM electrodes [35], however, in comparison with the other electrodes discussed below, the disk electrode still shows better potential values. A linear relationship between the peak current (I_p) and square root of scan rate (v) was observed, Fig. 7a (inset) confirming a diffusion controlled L-cysteine electrooxidation. The linear behavior of this plot was observed for both electrodes. A 23% current decrease was observed for cysteine oxidation on SAM of complex **1** on Au disk electrode, after the first scan Fig. 8a, thereafter the current stabilized. For complex **2** on Au disk electrode, there was a 32% decrease of the current before it stabilized, hence complex **1** shows better stability than **2**. The currents for cysteine oxidation on disk electrode could be regenerated to >62% by rinsing the electrode in pH 4 buffer.

Figure 7b shows electrocatalysis of cysteine oxidation using the SAM modified gold UMCE. At the concentration of 1×10^{-6} mol cm^{-3}, a crossing over of the cyclic voltammograms at about 0.6 V (for **1**-SAM) and 0.67 V (for **2**-SAM) was observed. This is due to passivation of the electrode by cysteine oxidation products. Decreasing the concentration to 1×10^{-7} mol cm^{-3} resulted in no passivation on both SAM modified electrodes (Fig. 7b, inset). However, for comparison purposes, the concentration of 1×10^{-6} mol cm^{-3} was chosen because it was found that at much lower concentrations (<1×10^{-7} mol cm^{-3}) there was no catalysis on the SAM modified fiber electrodes. This suggests that the CoPc SAMs on the fiber electrodes are not effective catalysts at low analyte concentrations. Cysteine oxidation (1×10^{-6} mol cm^{-3}) peaks were observed at 0.84 and 0.90 V for **1**-SAM and **2**-SAM modified UMCE respectively. The inset in Fig. 7b also shows that at lower concentrations catalysis occurred at the same potential (0.95 V) for both SAM modified electrodes and at higher potentials compared to higher concentrations. Thus **1**-SAM electrode shows better behavior in high concentrations than **2**-SAM electrode in that lower potential for cysteine oxidation is observed in the former. The cysteine catalysis on the UMCE occurs (0.84 and 0.90 V) at much higher

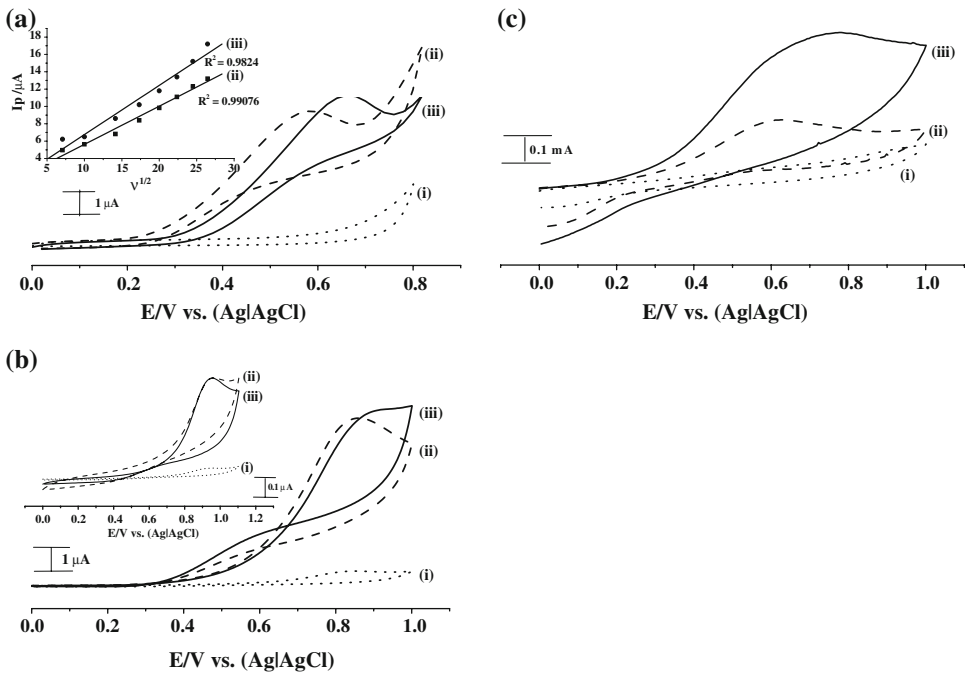

Fig. 7 Cyclic voltammograms of (i, dotted) unmodified gold disk electrode, (ii, dashed) SAM of complex **1** and (iii, solid) SAM of complex **2** in 1×10^{-6} mol cm^{-3} L-cysteine in pH 4 buffer solution. **a** Au disk electrodes, (**b**) Au UMCE and (**c**) Au fiber. Inset in (**a**): plots of square root of scan rate versus cysteine oxidation peak current for (i) SAM of complex **1** and (ii) SAM of complex **2**. Inset in (**b**) cyclic voltammogram of L-cysteine at low concentration (1×10^{-7} mol cm^{-3}). Scan rate = 50 mV s^{-1}

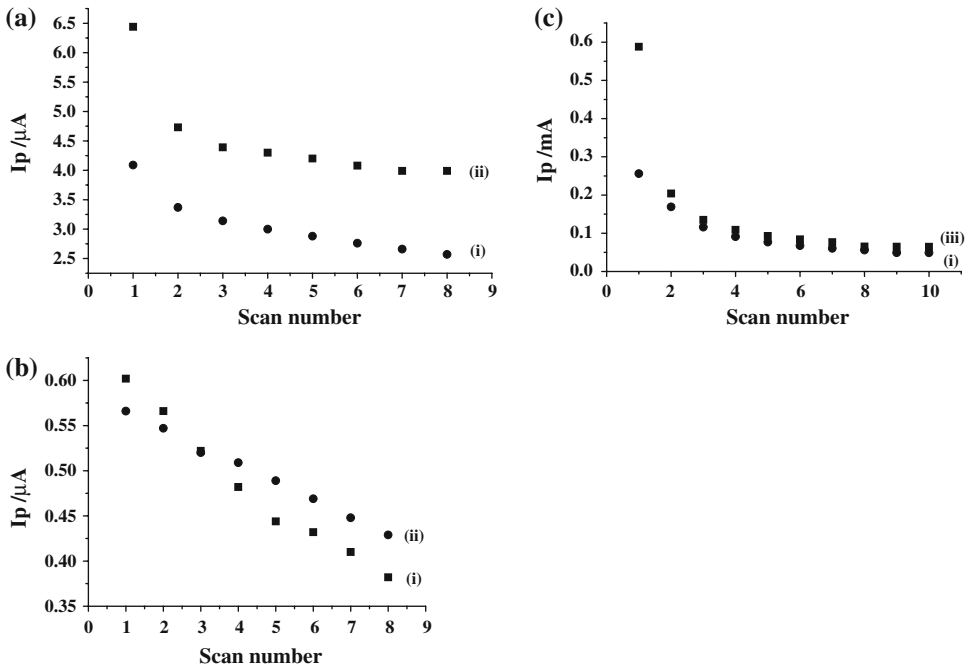

Fig. 8 Plot of I_p versus cyclic voltammetry scan number for the electrocatalytic oxidation of 1×10^{-6} mol cm^{-3} L-cysteine in pH 4 buffer on (i) SAM of complex **1** and (ii) SAM of complex **2**. **a** Au disk, (**b**) Au UMCE and (**c**) Au fiber

potentials compared to catalysis on the disk electrodes (0.55 and 0.65 V), showing that the latter are preferable for cysteine electrooxidation. Figure 8b shows that there was a continuous decrease in current with scan number for the oxidation of cysteine on SAMs of complexes **1** and **2** on Au UMCE showing that these electrodes are not stable. However, the electrodes could be regenerated (>80%) by rinsing in pH 4 buffer.

Figure 7c shows L-cysteine electrocatalytic oxidation on SAMs of complexes **1** and **2** on the gold coated fiber. Complex **2**-SAM shows a large increase in the catalytic current, with an oxidation potential of 0.77 V for cysteine oxidation, whereas catalysis with complex **1**-SAM gives an oxidation potential at 0.62 V for cysteine oxidation, but with lower catalytic currents. After the initial scan the gold coated fiber becomes passivated such that the catalytic peak becomes very weak for both SAMs of complexes **1** and **2**, Fig. 8c. The electrode could be regenerated to only 10% by rinsing in pH 4 buffer. However, it is important to note that large current (mA) were observed for the fiber compared to currents produced at the Au disk and Au UMCE (Fig. 7) bare electrodes (both in μA range). This is because the fiber is made of numerous micro strands. Thus even when the fiber is passivated, it still has higher currents than the Au disk and Au UMCE.

For all the electrodes, recovery occurs because when rinsing in pH 4 buffer, the oxidation product (cystine) which blocks the active sites on the electrode surface is removed in the process. Cystine is soluble in pH 4 buffer. The recovery process shows that the UMCE recovers best and the fiber hardly recovers at all.

Comparing the electrodes modified with complex **1** for cysteine oxidation shows that each Au electrode geometry has its advantages and disadvantages. Comparing Au disk and UMCE shows the former to have slightly higher currents (see starting currents in Fig. 8 for 1×10^{-6} mol cm^{-3} cysteine oxidation). In terms of cysteine oxidation overpotential Au disk outperforms the UMCE by having lower potential values. Also in terms of stability, the UMCE showed a continuous decrease in current with cyclic voltammetry scan number, whereas the disk stabilized after a 23 or 32 % decrease in current. Thus comparing Au disk and UMCE, the former is better for cysteine oxidation in terms of potential, starting current intensity and stability. The Au fiber gave much larger currents when compared to both the disk and the UMCE, but gave lower cysteine oxidation potential than UMCE and higher than the disk. However in terms of stability both the fiber and the UMCE performed worse than the disk. Thus in general in terms of overpotential and stability, the Au disk outperforms both the gold coated fiber and the UMCE.

Different overpotential reductions and current increases (sensitivity) were observed for the three electrodes, such differences in electrochemical behaviors suggest that electrocatalysis on the Au surfaces is largely influenced by electrode geometry and electrode size. Electrode geometry plays an important role in determining the type of diffusion on the electrode surface. The disk electrode experiences linear diffusion which suggest that there are less analytes coming to the electrode surface of the disk as compared to UMCE and fiber electrode where mass transport is enhanced due to the non-linear diffusion. This also explains

the intense passivation and high current densities experienced at the UMCE and fiber electrode. The fiber electrodes experienced much more increase in catalytic currents because the fiber is a bundle of many micro fiber strands.

The potential for cysteine oxidation will be directly related to the $Co^{III}Pc/Co^{II}Pc$ couple of the CoPc derivatives (**1** and **2**) since it is this couple which is known to catalyze cysteine oxidation in acid media [36]. This couple was observed at 0.3 V for **1** and 0.4 V for **2** in pH 4 buffer, for the Au disk (Fig. 3). For UMCE, the $Co^{III}Pc/Co^{II}Pc$ was observed as a very broad feature around 0.4 V for complex **1**, Fig. 4a. For the fiber, this couple was not clear since it was probably overlapped with peaks due to exposed gold oxide peaks. However it is clear that the lower potential value for cysteine oxidation on Au disk electrode SAMs for complex **1** is related to the low potential for the $Co^{III}Pc/Co^{II}Pc$ couple on this electrode. The ease of oxidation and hence the enhancement of the catalytic activity may be caused by the fact that non peripheral substitution enriches the electron density of the π conjugated ring.

Hydrodynamic experiments were carried out using a gold rotating disk electrode (RDE), Fig. 9 shows typical RDE curves obtained for cysteine oxidation on complex **1**-SAM and complex **2**-SAM modified electrode at 800 rpm. The inset shows the Levich plots, showing that the Levich equation is obeyed for both SAMs. The curves in Fig. 9 show complex **1** as the better catalyst since the foot of the wave occurs at less positive potentials compared to complex **2**. Thus RDE shows non-peripherally substituted complex **1** to be a better catalyst for cysteine oxidation. The corresponding Tafel slope values were obtained from the plot of E versus log I_k (Fig. 10), where $I_k = (I_m \times I_L)/(I_m - I_L)$. i_K is current when the system is under complete kinetics, i.e. analyte transport is governed by rotation of the electrode and not diffusion, i_L is limiting current (plateau in RDE voltammogram) and i_m is measured current and it has to be less than 5% of i_L. The values were found to be 173 and 199 for complex **1**-SAM and complex **2**-SAM modified electrodes, respectively. Such large Tafel slopes suggest strong substrate-ligand interaction [37–40]. The values of the Tafel slopes do however suggest that the first one electron transfer is rate determining, confirming the well-known mechanism for cysteine oxidation on CoPc complexes [36].

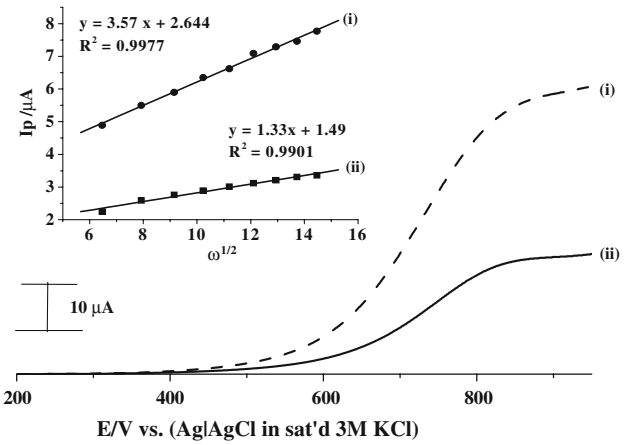

Fig. 9 Hydrodynamic voltammograms of L-cysteine (1×10^{-6} mol cm^{-3}) oxidation on SAM of complex **1** (i, dashed) and complex **2** (ii, solid) on Au disk electrode. Rotation rate 800 rpm scan rate 20 mV s^{-1}. Inset is the Levich plot for complex **1** (i) and complex **2** (ii)

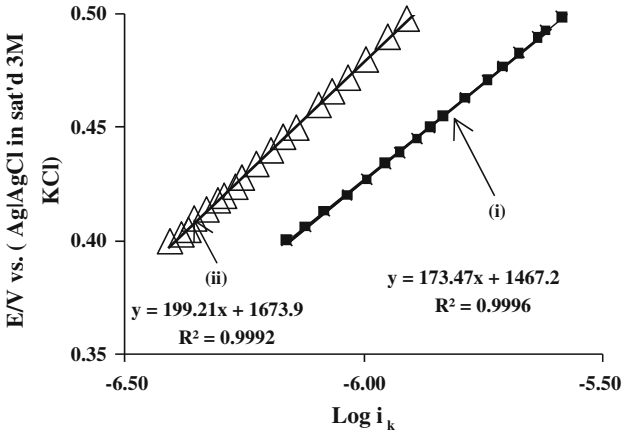

Fig. 10 Tafel plot for L-cysteine oxidation on SAM of complex **1**(i) and SAM of complex **2** (ii) for 1×10^{-6} mol cm^{-3} L-cysteine in pH 4 buffer solution

The values of the Tafel slope were similar to those obtained from cyclic voltammetry using Eq. 5, employed for irreversible-diffusion controlled catalytic reaction:

$$E_p = \frac{2.3RT}{2(1-\alpha)n_aF}\log \nu + K \quad (5)$$

where α is the transfer coefficient, n_a is the number of electrons involved in the rate determining step, ν is the scan rate, K is a constant and the remaining symbols have their usual meaning. From the plot of E_p versus log ν (Fig. 11), the SAM of complex **1** gave a Tafel slope of 173 mV/decade, and complex **2** gave 184 mV/decade, which are quite similar to those obtained from RDE experiments. Figure 12 shows a linear dependence of cysteine concentration on currents and the detection limits for cysteine analysis were determined using 3σ criterion and were of the order 10^{-7} M which is in the range as reported before [35].

4 Conclusions

Thio derivatised phthalocyanines (complexes **1** and **2**) were employed as self-assembled monolayers on a gold disk,

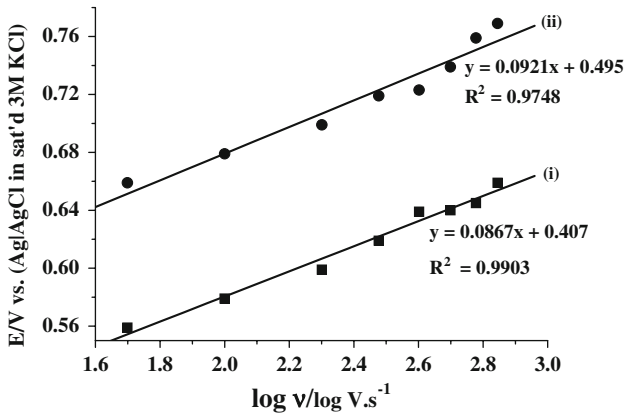

Fig. 11 Plot of E_p versus log v for the electrocatalytic oxidation of 1×10^{-6} mol cm^{-3} L-cysteine in pH 4 buffer on (i) complex **1** and (ii) complex **2**

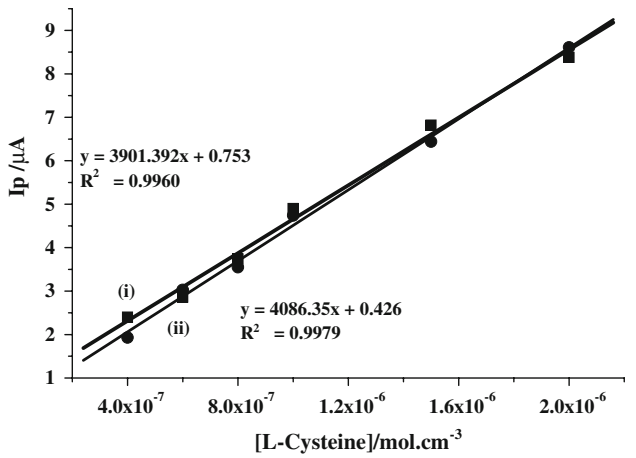

Fig. 12 Plot of I_p versus concentration for L-cysteine in pH 4 buffer on (i) SAM of complex **1** and (ii) and SAM complex **2**

gold UMCE and on a gold coated fiber. The SAMs were used for L-cysteine catalysis with complex **1** being the better catalyst than **2** in terms of RDE experiments which showed the foot of the wave for cysteine oxidation to occur at a lower potential for the former. Complex **1** is non-peripherally substituted with alkylthio groups while **2** is peripherally substituted with the same groups. The fact that complex **1** shows better catalytic behavior towards cysteine oxidation, may suggest that non-peripheral substitution may enhance catalytic activity. The extent of regeneration of the catalyst on the electrode surface as well as the stability of the catalyst on the disk electrode makes these simple SAM modified electrodes attractive for the development of potential thiol chemical sensors.

Acknowledgements This work was supported by the Department of Science and Technology (DST) and National Research Foundation (NRF), South Africa through DST/NRF South African Research Chairs Initiative for Professor of Medicinal Chemistry and Nanotechnology and Rhodes University and by BOF from Ghent University through a BOF-Flanders/NRF-South Africa research project. NN thanks Andrew Mellon Foundation and NRF for a bursary and Flanders/NRF bilateral agreement for a travel grant to Belgium.

References

1. Guillaud S, Germain JP (1998) Coord Chem Rev 180:1433
2. Collins RA, Mohammed KA (1988) J Phys D Appl Phys 21:154
3. Zagal J, Bedioui F, Dodelet JP (eds) (2006) N4-macrocyclic metal complexes. Springer, New York
4. McKeown N (1992) Chem Ind 92
5. Duro AJ, de la Torre G, Barber J, Serrano JL, Torres T (1996) Chem Mater 8:106
6. Classens CG, Blau WJ, Cook M, Hanack M, Nolte RJM, Torres T, Wöhrle D (2001) Monatsh Chem 132:3
7. de la Torre G, Vasquez P, Agull′o-L′opez F (1997) Adv Mater 9:265
8. de la Torre G, Vaquez P, Agull′o-L′opez F, Torres T (1998) J Mater Chem 8:1671
9. Allen CM, Sharman WM, van Lier JE (2001) J Porphyrins Phthalocyanines 5:1
10. Bonnett R (2000) In: Chemical aspects of photodynamic therapy, Gordon and Breach Science, Canada
11. Gregory P (2000) J Porphyrins Phthalocyanines 4:432
12. Martin CR, Foss CA (1996) In: Kissinger PT, Heineman WR (eds) Laboratory techniques in electroanalytical chemistry, 2nd edn. Marcel Dekker Inc., New York (Chap. 13)
13. Porter MD, Bright TB, Allara DL, Childsey CED (1987) J Am Chem Soc 109:3559
14. Chaki NK, Aslam M, Sharma J, Vjayamohanan K (2001) Proc Indian Acad Sci (Chem Sci) 113:689
15. Bard AJ, Faulkner LR (2001) In: Electrochemical methods fundamentals and applications, 2nd edn. John Wiley & Sons Inc.
16. Amatore C (1995) In: Stein IR (ed) Physical electrochemistry principles, methods and applications. Marcel Dekker Inc. Chap. 4
17. Bagotsky VS (2006) In: Fundamentals of electrochemistry, 2nd edn. John Wiley & Sons Inc.
18. Michael AC, Wightman RM (1996) In: Kissinger PT, Heineman WR (eds) Laboratory techniques in electroanalytical chemistry. Marcel Dekker Inc. Chap. 12
19. Westbroek P, Priniotakis G, Kiekens P (2005) In: Analytical electrochemistry in textiles. Woodhead Publishing Limited
20. Nombona N, Nyokong T (2009) Dyes Pigments 80:130
21. Heatfield MT, Fearn S, Sterenton GB, Waring AC, Sturman SG (1990) Neurosci Lett 110:216
22. Cengiz M, Yuksel A, Seven M (2000) Pharmacol Res 41:423
23. Ebadi M, Srinivason SK, Baxi MD (1996) Prog Neurobiol 48:1
24. Bald E, Kaniowska E, Chwatko G, Glowacki R (2000) Talanta 50:1233
25. Ueland PM, Mansoor MA, Guttormsen AB, Muller F, Aukrust P, Refsum H, Svardal AM (1996) J Nutr 126:1281
26. Gasana E, Westbroek P, Hakuzimana J, De Clerck K, Priniotakis G, Kiekens P, Tseles D (2006) Surf Coat Tech 201:3547
27. Schwarz A, Hakuzimana J, Gasana E, Westbroek P, Van Langenhove L (2007) Gold coated yarns: a material for endurance. In Proceedings ITMC, Casablanca, Morocco
28. Caro CA, Bedioui F, Zagal JH (2002) Electrochim Acta 47:1489
29. Agboola B, Ozoemena KI, Westbroek P, Nyokong T (2007) Electrochem Commun 9:310
30. Claußen A, Ochoa G, Páez M, Costamagna J, Nyokong T, Bedioui F, Zagal JH (2008) J Solid State Electrochem 12:473
31. Griveau S, Pavez J, Zagal JH, Bedioui F (2001) J Electroanal Chem 497:75

32. Li Z, Lieberman M, Hill W (2001) Langmuir 17:4887
33. Pilloud DL, Chen X, Dutton P, Moser CC (2000) J Phys Chem 104:2868
34. Khene S, Geraldo DA, Togo CA, Limson J, Nyokong T (2008) Electrochim Acta 54:183
35. Ozoemena K, Nyokong T (2002) Electrochim Acta 47:4035
36. Maree S, Nyokong T (2000) J Electroanal Chem 492:120
37. Wermeckers B, Beck F (1985) Electrochim Acta 30:1491
38. Lyons MEG, Fitzgerald CA, Smyth MR (1994) Analyst 119:855
39. Zen J-M, Senthil Kumar A, Chang M-R (2000) Electrochim Acta 45:1691
40. Sethlotho N, Nyokong T, Zagal JH, Bedioui F (2006) Electrochim Acta 51:5125